HHS Public Access

Author manuscript

Angew Chem Int Ed Engl. Author manuscript; available in PMC 2014 June 10.

Published in final edited form as:

Angew Chem Int Ed Engl. 2013 June 10; 52(24): 6190–6195. doi:10.1002/anie.201302245.

Multimodal magnetic core-shell nanoparticles for effective stem cell differentiation and imaging**

Birju Shah,

Department of Chemistry & Chemical Biology, Institute for Advanced Materials, Devices and Nanotechnology (IAMDN), Rutgers, The State University of New Jersey, Piscataway, NJ 08854, USA

Perry T. Yin, and

Department of Biomedical Engineering, Rutgers, The State University of New Jersey, Piscataway, NJ 08854 (USA)

Ki-Bum Lee*

Department of Chemistry & Chemical Biology, Institute for Advanced Materials, Devices and Nanotechnology (IAMDN), Rutgers, The State University of New Jersey, Piscataway, NJ 08854, USA

Keywords

neural stem cells; magnetic core-shell nanoparticles; stem cell differentiation; siRNA delivery; magnetically-facilitated delivery

Stem cells, owing to their ability to differentiate into specialized cells that can serve a particular function, have enormous potential in the field of regenerative medicine, wherein these stem cell-based therapies can be used to treat a wide range of diseases including diabetes, heart disease, and liver disease.[1] However, the realization of stem cell-based therapies in the clinic is severely hampered by our current inability to achieve the efficient delivery of genetic materials into target cells, which is required to specifically direct differentiation. In particular, with regard to stem cell-based regenerative medicine, it is vital to achieve: i) the highly efficient transfection of targeted cells; ii) biocompatibility, with an emphasis on maintaining a high cell viability without altering migratory and differentiation potential; and iii) non-invasive monitoring for the long-term evaluation of therapy.[2]

Currently, the use of virus-mediated delivery results in the highest delivery efficiency (80–90%) for stem cells.[3] However, this method also has a number of harmful effects that limit its clinical applicability including potential cell toxicities, mutagenesis, and the induction of an immune response.[4] To this end, a significant amount of effort has been invested in the development of alternative non-viral delivery methods.[2c] In particular, recent studies have

**This work was financially supported by the NIH Director's Innovator Award [(1DP20D006462-01), K.B. Lee] and the N.J. Commission on Spinal Cord grant [(09-3085-SCR-E-0), K.-B. Lee]. P.T. Yin would like to acknowledge NIH Biotechnology Training Grant for their support. We would like to thank Shraboni Ghoshal for help in synthesis and Prasad Subramaniam and Nicholas Pasquale for their useful comments on the manuscript.

*kblee@rutgers.edu, Homepage:http://rutchem.rutgers.edu/~kbleeweb/.

demonstrated that magnetic nanoparticles (MNPs) possess a number of advantages that are especially attractive for application to stem cell research.[5] Typically, MNPs are composed of a magnetic core that can consist of metals or metal oxides,[6] metal alloys,[7] and more recently, doped metals.[8] These MNP cores can then be post-synthetically modified with a biocompatible material (e.g. SiO_2, gold, polymer, etc) resulting in a core-shell structure.[9] In doing so, this shell can not only act as a hydrophilic layer but also as a platform for the surface functionalization of the MNPs.[10] As a result of its inherent magnetism, the properties of the shell, and the surface functionalization employed, MNPs can possess multifunctionalities including the delivery of nucleic acids such as plasmid DNA (pDNA) and short interfering RNA (siRNA), magnetically-facilitated delivery, cell targeting, and MRI contrast.[11] In particular, the synthesis of gold coated MNPs can provide a number of additional advantages such near-infrared (NIR) absorption,[12] photon scattering, and a relatively inert and facile surface that is amenable to further functionalization, while preserving the core magnetic properties.[13]

Herein, we describe the synthesis of well-defined magnetic core-shell nanoparticles [MCNPs], composed of a highly magnetic core surrounded by a thin uniform gold shell and their application for the delivery of genetic materials (siRNA and pDNA) into stem cells in a highly efficient, spatiotemporally controlled, and biocompatible manner (Figure 1). Moreover, we demonstrate the utility of the multifunctionalities that are provided by our MCNP system including magnetically-facilitated transfection and dark-field imaging. While numerous studies have previously utilized MNPs as MRI contrast agents and have shown the effectiveness of magnetically facilitated transfection in stem cells, the use of MCNPs to mediate the delivery of genetic materials to stem cells in a highly efficient and biocompatible manner remains to be assessed. To this end, as a proof-of-concept experiment for the genetic manipulation of stem cells using MCNPs and the accompanying differentiation studies, neural stem cells (NSCs) were chosen as they are known to be very sensitive to conventional exogenous lipid-based transfection reagents as well as difficult-to-transfect.[2a] Specifically, we hypothesized that we could achieve a significantly higher transfection efficiency for genetic materials without compromising stem cell viability and biological functions (e.g. differentiation) using our MCNP-based magnetically-facilitated delivery. In addition, we hypothesized that the gold shell would provide additional advantages for stem cell-based therapies through the ability to perform dark field imaging, as this would be a simple method with which to confirm the presence of MCNPs within stem cells prior to transplantation or other studies.

For the formation of our MCNPs, we chose doped magnetic nanoparticles ($ZnFe_2O_4$) as our core, since these MNPs have been shown to have a significantly higher magnetic susceptibility and hence can afford improved magnetic properties at much lower concentrations when compared to conventional MNPs.[8] As such, we first synthesized these $ZnFe_2O_4$ NPs via the thermal decomposition of a mixture of metal precursors in the presence of oleic acid as a stabilizer, using a modified synthetic protocol that was previously reported.[8] These $ZnFe_2O_4$ NPs were then coated with a thin layer of Au by reducing hydrogen tetrachloroaurate hydrate ($HAuCl_4.3H_2O$) in a chloroform solution of oleylamine in the presence of $ZnFe_2O_4$ NPs, which resulted in the formation of non-water-soluble MCNPs (Figure 1A).[14] These non-water-soluble $ZnFe_2O_4$@Au nanoparticles were then

rendered water-soluble by exchanging their surface oleylamine moieties with 11-mercaptoundecanoic acid (MUA).[15] Initial characterization was performed to confirm that the water-soluble MCNPs (Figure 1A) retained their magnetic properties (Figure 2D) and showed a distinct pink coloration, which resembles a gold colloidal solution (Figure 2E), due to the surface plasmon resonance (SPR) properties of the outer Au shell.

A detailed characterization of the as-synthesized MCNPs ($ZnFe_2O_4$@Au NPs) was then performed. First, transmission electron microscopy (TEM) analysis revealed that the overall diameter increased from 20 ± 1.2 nm (n=100) for the $ZnFe_2O_4$ MNPs (See supporting information, Figure S1) to 25 ± 2.7 nm (n=100) for the $ZnFe_2O_4$@Au NPs (Figure 2A). The lattice fringes in the Au shell can clearly be seen in the HRTEM (Figure 2B), and the interfringe spacing was measured to be 0.201 nm, which is the interplane distance of the (200) planes in the face centered cubic (fcc) Au. This indicates that the $ZnFe_2O_4$ nanoparticles are indeed coated with a layer of crystalline Au (~2.5 nm). Furthermore, from the HRTEM images (Figure 2B), we observed a difference in the contrast between the darker $ZnFe_2O_4$ core and the lighter Au shell. It has been reported that this is attributed to the dominance of the mass contrast over the diffraction contrast, making Au appear lighter in spite of it having a higher electron density than Fe and Zn.[16] We also confirmed that the MCNPs were composed of Zn, Fe, and Au using Energy Dispersive X-Ray Spectroscopy (EDAX) analysis (Figure 2C). Finally, from the UV absorption data (Figure 2F), we clearly observed that the water-soluble MCNPs show a distinct absorption peak at 540 nm, owing to the SPR properties of the water-soluble Au nanostructures. As expected, this peak is not observed in both the core $ZnFe_2O_4$ MNPs and the non-water-soluble $ZnFe_2O_4$@Au NPs coated with oleylamine.

To prepare these aforementioned MCNP constructs for the delivery of functional genetic materials such as siRNAs or pDNAs, the water-soluble MCNPs were coated with a cationic polyamine-dendrimer that was previously developed by our group[17] (Figure 1A; See supporting information, Figure S2) to afford an overall positive charge to the MCNPs. This positive charge facilitated MCNP complexation with negatively charged siRNA or pDNA. In addition, the cationic polyamine-dendrimer has multiple primary amine groups and hence, once the MCNP constructs are internalized, it can act as a proton sponge in the endosomes, thereby aiding in subsequent endosomal escape of the complexes and protecting the cargo from the deleterious effects of the acidic microenvironment.[17] The hydrodynamic size of the final MCNP constructs was determined to be 70 ± 2 nm and their net surface charge was found to be +15 mV using dynamic light scattering (DLS) and zeta potential measurements, respectively (See supporting information, Figure S3). Additionally, we determined the amount of siRNA bound to the positively charged MCNPs at different concentrations using Picogreen assay (See supporting information, Figure S4).

Once we finished optimizing the synthesis of the MCNP constructs, we tested whether the MCNPs and/or the use of magnetically-facilitated delivery negatively affect the intrinsic ability of NSCs to proliferate and differentiate. To accomplish this, we assessed the proliferation and differentiation capabilities of the NSCs following their exposure to increasing concentrations of MCNPs (2~20 μg/mL) (See supporting information, Figure S5) that are complexed with negative control siRNA either in the presence or absence of an

external magnetic field (MF), using immunocytochemistry. Based on the expression of proliferation (Ki67) and differentiation (TUJ1 for neurons and GFAP for glial cells) markers, we were able to ascertain that the intrinsic biological functions of the NSCs were unaffected by our MCNPs and the delivery methods employed (Figure 3A). Since we confirmed the excellent biocompatibility and non-toxicity of our MCNPs in NSCs, we went ahead and tested the capability of these MCNPs to translocate genetic materials (siRNA or pDNA) into NSCs-GFP, which are genetically labeled with green fluorescent protein (GFP), in the presence or absence of an external MF and compared to commercially available transfection agents such as X-tremeGENE®. To this end, we first identified the optimal external MF exposure time that results in maximum transfection efficiency while preventing deleterious effects to cell viability (See supporting information, Figure S6). To accomplish this, we complexed the MCNPs with Cy3-labeled control siRNA (red color, Silencer®, Ambion) and incubated these complexes with NSCs-GFP in the presence of a MF for increasing periods of time (ranging from 0 to 6 h). After each exposure time point, the NSCs-GFP were washed with DPBS three times to remove untransfected MCNP-siRNA constructs. Using fluorescence microscopy, we observed a sharp increase in the uptake and localization of the tested MCNP-siRNA constructs (Figure 3B) into the cytoplasm of the NSCs-GFP after the complexes were incubated with the NSCs for only 30 min in the presence of a MF, as compared to control (Figure 3B). Upon increasing the time of incubation, we observed a minimal increase in the uptake and localization of MCNP-siRNA constructs See (supporting information, Figure S7). As such, we subsequently identified 30 min as the optimum MF exposure time to offset any deleterious effects to the NSCs-GFP and used this for all of the following experiments.

Next, to demonstrate the delivery of functional MCNP-siRNA constructs, we chose siRNA against GFP (siGFP) and optimized the concentrations of MCNP and siGFP to be delivered by varying their respective concentrations and measuring the resulting GFP knockdown efficiency (See supporting information, Figure S8). Once we identified the optimum concentrations of MCNP (5 μg/ mL) and siGFP (200 nM), we compared the knockdown efficiency of MCNPs-based trasfection with that of the commercial transfection agent, X-tremeGENE®. Specifically, the X-tremeGENE® was complexed with the same concentration of siRNA (200 nM) in the ratio of 3:1 as recommended by the manufacturer. To this end, the MCNP-siGFP and X-tremeGENE®-siGFP constructs were incubated with NSCs-GFP for increasing periods of time (from 15 min to 6 h), to first elucidate the correlation between the incubation time and the transfection efficiency, wherein we used the optimized MF exposure time (30 min) for all conditions. For comparison, we used the recommended incubation time (6 h) for the commercially available transfection reagents (e.g. X-tremeGENE®). After each period of incubation, the cells were washed with DPBS three times and further incubated for a period of 72 h, following which we quantified the decrease in the GFP signal intensity of the NSCs. We saw a significant difference in the gene silencing capability of MCNPs in the presence of a MF (55.45 % knockdown, $p < 0.01$) as compared to that in the absence of a MF (36.75% knockdown) (Figure 3C), when the complexes were incubated for 6 h. Additionally, upon comparison of our magnetically-facilitated delivery with X-tremeGENE®-based delivery, we observed a remarkable difference in the time-dependent progression curve of the transfection efficiency (Figure 3D)

and in the cytotoxic effects exhibited by the two experimental conditions (See supporting information, Figure S9). In the case of magnetically-facilitated delivery (MCNP-siGFP/MF, Figure 3D), significantly higher levels of GFP knockdown (45.6% knockdown, $p < 0.01$) were observed after only 15 min of incubation with negligible cytotoxicity (~97% cell viability; See supporting information, Figure S9). Moreover, an additional increase in the gene silencing was seen after increasing the incubation time to 6h (55.45% knockdown). In contrast, negligible GFP knockdown was seen in the case of X-tremeGENE®-siGFP complexes after 15 min of incubation, which gradually increased upon increasing the incubation time, and reaches a plateau (38.95% knockdown, Figure 3D) after 6h, however, with significant cytotoxicity (60% cell viability; $p < 0.01$, See supporting information, Figure S9). From the analysis of the GFP knockdown results (Figure 3D), we identified 30 min as the optimum incubation period needed to achieve significant downstream effects from gene delivery using MCNP/MF.

To see whether we could increase transfection efficiency further, we carried out repeated transfections of the same cell culture (a technique known as multifection[18]) using our MCNP/siGFP constructs and compared the gene-silencing efficiency achieved with multifection to that of a single transfection. We found that we were able to further improve the gene silencing efficiency from 55% (single transfection of MCNP/siGFP) to 65% (multifection of MCNP/siGFP) (See supporting information, Figure S10a). In the case of X-tremeGENE multifection, we observed a similar trend of increased GFP knockdown (45% for multifection vs. 38% for single transfection). However, upon comparing their toxicity profiles, the viability of cells multi-transfected with MCNPs only decreased slightly ($p > 0.05$ as compared to control), while that of X-tremeGENE resulted in significant cell death ($p < 0.01$ as compared to control, See supporting information, Figure S10b). Finally, besides siRNA, we also demonstrated the delivery of plasmid DNA (DsRED) to NSCs-GFP using our MCNPs under similar experimental conditions as compared to siRNA delivery. The magnetically-facilitated delivery of MCNP-DsRED complexes led to significantly higher levels of gene expression in NSCs within a shorter incubation time as compared to delivery of the same complexes in the absence of a MF (See supporting information, Figure S11). Thus, we observed that in spite of shorter-than commonly used incubation times, highly efficient gene deactivation (in the case of siGFP, Figure 3) or activation (in the case of DsRED; See supporting information, Figure S11) was achieved with negligible toxicity when magnetically-facilitated delivery of MCNP constructs was utilized, which is in contrast to that seen with the positive control experiments using standard transfection agents under the same conditions. However, to achieve comparable levels of knock-down results using the aforementioned lipid-based transfection methods, we typically needed longer incubation times (>6h), which can induce significant cytotoxic effects resulting in a low cell viability (~60% cell viability).

**This work was financially supported by the NIH Director's Innovator Award [(1DP20D006462-01), K.B. Lee] and the N.J. Commission on Spinal Cord grant [(09-3085-SCR-E-0), K.-B. Lee]. P.T. Yin would like to acknowledge NIH Biotechnology Training Grant for their support. We would like to thank Shraboni Ghoshal for help in synthesis and Prasad Subramaniam and Nicholas Pasquale for their useful comments on the manuscript.

Having demonstrated that our MCNPs, in the presence of a MF, can efficiently manipulate gene expression in NSCs without compromising their biological functions, we focused on controlling the neural differentiation of NSCs using our optimized conditions (Figure 4A) in order to demonstrate the utility of our MCNPs for stem cell-based therapies. For this demonstration, we selected functional siRNAs targeting key genes such as *CAVEOLIN-1* (si*CAV*)[19] or *SOX9* (si*SOX9*)[20] (Figure 4A). These two genes (*CAVEOLIN-1* and *SOX9*) have already been identified as "neural switches" that, when inhibited, selectively control the differentiation of NSCs into oligodendrocytes and neurons, respectively. To demonstrate the effective genetic manipulation of NSCs to control their differentiation, the MCNP-siRNA complexes (MCNP, 5 μg/mL; si*CAV*/si*SOX9*, 200 nM) were prepared and incubated with NSCs in the presence of a MF (t = 30 min) as optimized previously. Untreated NSCs and NSCs treated with MCNP-siRNA constructs were characterized and quantified using immunocytochemistry by staining for oligodendrocytes [myelin binding protein (MBP)] and neuron [β-tubulin (TUJ1)] markers at day 7 after transfection (Figure 4B). From these experiments, we observed a significant increase in the percentage of oligodendrocytes (MBP-positive) and neurons (TUJ1-positive) in the cells treated with si*CAV* or si*SOX9* respectively, as compared to the spontaneous differentiation condition (Figure 4C, $p < 0.01$ for si*CAV* and $p < 0.001$ for si*SOX9* treatment). Thus, using the magnetically-facilitated delivery of MCNP-siRNA constructs, we were able to control the differentiation of NSCs to a particular lineage to a significantly greater extent and within shorter incubation periods, as compared to the untreated control NSCs. Finally, as this is the first report of using MCNPs to delivery genetic materials to NSCs, we investigated the cellular uptake mechanism of our magnetically-facilitated delivery of MCNPs into NSCs by treating the NSCs with endocytosis inhibitors and then quantifying their gene silencing effect. From this study, we were able to confirm that the cellular uptake occurred via a combination of clathrin-as well as caveolae-mediated endocytosis, which was similar to that of standard X-tremeGENE®-based and MNP-based transfection (See supporting information, Figure S12).

Finally, to demonstrate the multifunctional advantages that a gold shell can have for MCNP-based delivery of genetic materials and for stem cell-based therapies, we used dark imaging to confirm the uptake of the MCNPs into NSCs. As our MCNPs possess a thin gold shell and display surface plasmon resonance at 540 nm (Figure 2F), they can be used as cellular imaging modalities with simple dark-field microscopy. In particular, gold nanoparticles are known to scatter visible and infrared light owing to their localized surface plasmons.[21] In addition, they are significantly brighter than chemical fluorophores and do not photobleach, thus making them excellent candidates for biological imaging.[22] To this end, we studied the light scattering properties of our MCNPs complexed with control siRNA, by incubating them with NSCs and then monitored their intracellular uptake using a dark-field microscope. As seen in Figure 4D, the MCNPs scatter the incident white light more intensely as compared to the control cells. On the other hand, no noticeable change was seen when the cells were incubated with the magnetic core nanoparticles. Thus, besides improving the solubility and affording facile surface functionalization, the gold shell on our MCNPs can also be used as an imaging modality to confirm the localization of MCNPs to stem cells before further study or application. Also, owing to presence of the magnetic core, our MCNPs can afford MRI imaging capability as can be seen from Figure 4E providing further

advantages for *in vivo* applications.[8] To evaluate whether our MCNP retain their functions as an MRI contrast agent, we carried out MRI studies using MCNPs in phantom agar gels. Increasing the concentration of the MCNPs from 2 μg/ml to 50 μg/ml, led to a significant reduction in T_2, as evident from the decreased signal intensity. Additionally, this decrease was comparable to that of just the core NPs indicating that the Au shell does not negatively affect the MRI contrast of the core. These results, thus demonstrate that our MCNPs could also function as an MRI contrast agent due to shortening of T_2 relaxation and higher T_2 relaxivity.

In conclusion, we have synthesized magnetic core-shell nanoparticles (MCNPs) consisting of a highly magnetic $ZnFe_2O_4$ core surrounded by a gold outer-shell ($ZnFe_2O_4$@Au) and utilized them for the genetic manipulation of neural stem cells (NSCs) in a highly efficient, biocompatible, and spatiotemporally controlled manner. As a proof-of-concept for the utility of the MCNPS in the genetic manipulation of stem cells, we demonstrated that we could direct the differentiation of NSCs to specific lineages (neurons and oligodendrocytes) using our developed MCNPs to delivery siRNA. In particular, while MCNPs have been utilized for the highly efficient labeling of stem cells, this is the first demonstration that utilized MCNPs for the delivery of genetic materials (e.g. siRNA and pDNA) to stem cells. Moreover, these MCNPs hold a number of advantages for use with stem cell-based applications owing to multifunctionalities that result from the composite of the magnetic core with the gold outer-shell. In particular, we have demonstrated that the gold outer-shell i) enables a facile surface for the functionalization of our MCNPs with a cationic polyamine-dendrimer thereby allowing for the complexation of the MCNs with negatively charged genetic materials, ii) enhances biocompatibility of the MCNP with stem cells, and iii) allows for the use of a simple method with which to confirm the presence of MCNPs within stem cells through dark field imaging. In addition, previous studies have shown that a gold outer-shell improves aqueous solubility and long-term stability of the MCNPs. On the other hand, we have demonstrated that the magnetic core of the MCNP i) retains its excellent magnetic properties even after the formation of the gold outer-shell, ii) allows us to deliver nanoparticle-biomolecule constructs into the difficult-to-transfect stem cells with high transfection efficiency and with significantly shorter incubation times as compared to the conventional lipid-based transfection agents, and iii) can be used as an MRI contrast agent, which can be used in the future to track MCNP-transfected stem cells *in vivo*. Thus, MCNP-based genetic manipulation method can potentially be a powerful tool for stem cell applications.

Experimental Section

All experimental details and protocols are provided in the Supporting Information.

Supplementary Material

Refer to Web version on PubMed Central for supplementary material.

References

1. a) Fuchs E, Tumbar T, Guasch G. Cell. 2004; 116:769. [PubMed: 15035980] b) Reya T, Morrison SJ, Clarke MF, Weissman IL. Nature. 2001; 414:105. [PubMed: 11689955] c) Gimble JM, Katz AJ, Bunnell BA. Circ. Res. 2007; 100:1249. [PubMed: 17495232] d) Gurtner GC, Werner S, Barrandon Y, Longaker MT. Nature. 2008; 453:314. [PubMed: 18480812] e) Murry CE, Keller G. Cell. 2008; 132:661. [PubMed: 18295582]
2. a) Lakshmipathy U, Pelacho B, Sudo K, Linehan JL, Coucouvanis E, Kaufman DS, Verfaillie CM. Stem Cells. 2004; 22:531. [PubMed: 15277699] b) Solanki A, Kim JD, Lee K-B. Nanomedicine. 2008; 3:567. [PubMed: 18694318] c) Ferreira L, Karp JM, Nobre L, Langer R. Cell Stem Cell. 2008; 3:136. [PubMed: 18682237]
3. a) Zhang XY, La Russa VF, Bao L, Kolls J, Schwarzenberger P, Reiser J. Mol. Ther. 2002; 5:555. [PubMed: 11991746] b) Ma Y, Ramezani A, Lewis R, Hawley RG, Thomson JA. Stem Cells. 2003; 21:111. [PubMed: 12529558]
4. Pack DW, Hoffman AS, Pun S, Stayton PS. Nat. Rev. Drug Disc. 2005; 4:581.
5. a) Sapet C, Laurent N, de Chevigny A, Le Gourrierec L, Bertosio E, Zelphati O, Beclin C. Biotechniques. 2011; 50:187. [PubMed: 21486240] b) Chien L-Y, Hsiao J-K, Hsu S-C, Yao M, Lu C-W, Liu H-M, Chen Y-C, Yang C-S, D-M Huang. Biomater. 2011; 32:3275.c) Jenkins SI, Pickard MR, Granger N, Chari DM. ACS Nano. 2011; 5:6527. [PubMed: 21721568]
6. Hyeon T. Chem. Commun. 2003:927.
7. a) Park JK, Jung J, Subramaniam P, Shah BP, Kim C, Lee JK, Cho JH, Lee C, Lee KB. Small. 2011; 7:1647. [PubMed: 21560243] b) Seo WS, Lee JH, Sun X, Suzuki Y, Mann D, Liu Z, Terashima M, Yang PC, McConnell MV, Nishimura DG, Dai H. Nat. Mater. 2006; 5:971. [PubMed: 17115025]
8. Jang JT, Nah H, Lee JH, Moon SH, Kim MG, Cheon J. Angew. Chem. Int. Ed. 2009; 48:1234.
9. a) Wang LY, Park HY, Lim SII, Schadt MJ, Mott D, Luo J, Wang X, Zhong CJ. J. Mater. Chem. 2008; 18:2629.b) Tassa C, Shaw SY, Weissleder R. Acc. Chem. Res. 2011; 44:842. [PubMed: 21661727] c) Huang J, Bu LH, Xie J, Chen K, Cheng Z, Li XG, Chen XY. ACS Nano. 2010; 4:7151. [PubMed: 21043459] d) Zhao WR, Gu JL, Zhang LX, Chen HR, Shi JL. J. Am. Chem. Soc. 2005; 127:8916. [PubMed: 15969545]
10. Laurent S, Forge D, Port M, Roch A, Robic C, Elst LV, Muller RN. Chem. Rev. 2008; 108:2064. [PubMed: 18543879]
11. a) Chaudhuri RG, Paria S. Chem. Rev. 2012; 112:2373. [PubMed: 22204603] b) Zhang HY, Lee MY, Hogg MG, Dordick JS, Sharfstein ST. ACS Nano. 2010; 4:4733. [PubMed: 20731451]
12. a) Wang S, Chen K-J, Wu T-H, Wang H, Lin W-Y, Ohashi M, Chiou P-Y, Tseng H-R. Angew. Chem. Int. Ed. 2010; 49:3777.b) Jin YD, Jia CX, Huang SW, O'Donnell M, Gao XH. Nat Commun. 2010; 1
13. Xu C, Xie J, Ho D, Wang C, Kohler N, Walsh EG, Morgan JR, Chin YE, Sun S. Angew. Chem. Int. Ed. 2008; 47:173.
14. Xu Z, Hou Y, Sun S. J. Am. Chem. Soc. 2007; 129:8698. [PubMed: 17590000]
15. Guo S, Huang Y, Jiang Q, Sun Y, Deng L, Liang Z, Du Q, Xing J, Zhao Y, Wang PC, Dong A, Liang X-J. ACS Nano. 2010; 4:5505. [PubMed: 20707386]
16. a) Robinson I, Tung LD, Maenosono S, Waelti C, Thanh NTK. Nanoscale. 2010; 2:2624. [PubMed: 20967339] b) Ban ZH, Barnakov YA, Golub VO, O'Connor CJ. J. Mater. Chem. 2005; 15:4660.
17. Kim C, Shah BP, Subramaniam P, Lee K-B. Mol. Pharm. 2011; 8:1955. [PubMed: 21793576]
18. Pickard MR, Barraud P, Chari DM. Biomater. 2011; 32:2274.
19. Li Y, Lau W-M, So K-F, Tong Y, Shen J. Neurochem. Int. 2011; 59:114. [PubMed: 21693146]
20. a) Wegner M, Stolt CC. Trends Neurosci. 2005; 28:583. [PubMed: 16139372] b) Stolt CC, Lommes P, Sock E, Chaboissier MC, Schedl A, Wegner M. Genes Dev. 2003; 17:1677. [PubMed: 12842915] c) Solanki A, Shah S, Yin PT, Lee K-B. Sci. Rep. 2013; 3:1553. [PubMed: 23531983]
21. a) El-Sayed MA. Acc. Chem. Res. 2001; 34:257. [PubMed: 11308299] b) Murphy CJ, Gole AM, Stone JW, Sisco PN, Alkilany AM, Goldsmith EC, Baxter SC. Acc. Chem. Res. 2008; 41:1721. [PubMed: 18712884]

22. Jain PK, Huang XH, El-Sayed IH, El-Sayed MA. Acc. Chem. Res. 2008; 41:1578. [PubMed: 18447366]

cells prior to transplantation or other studies.

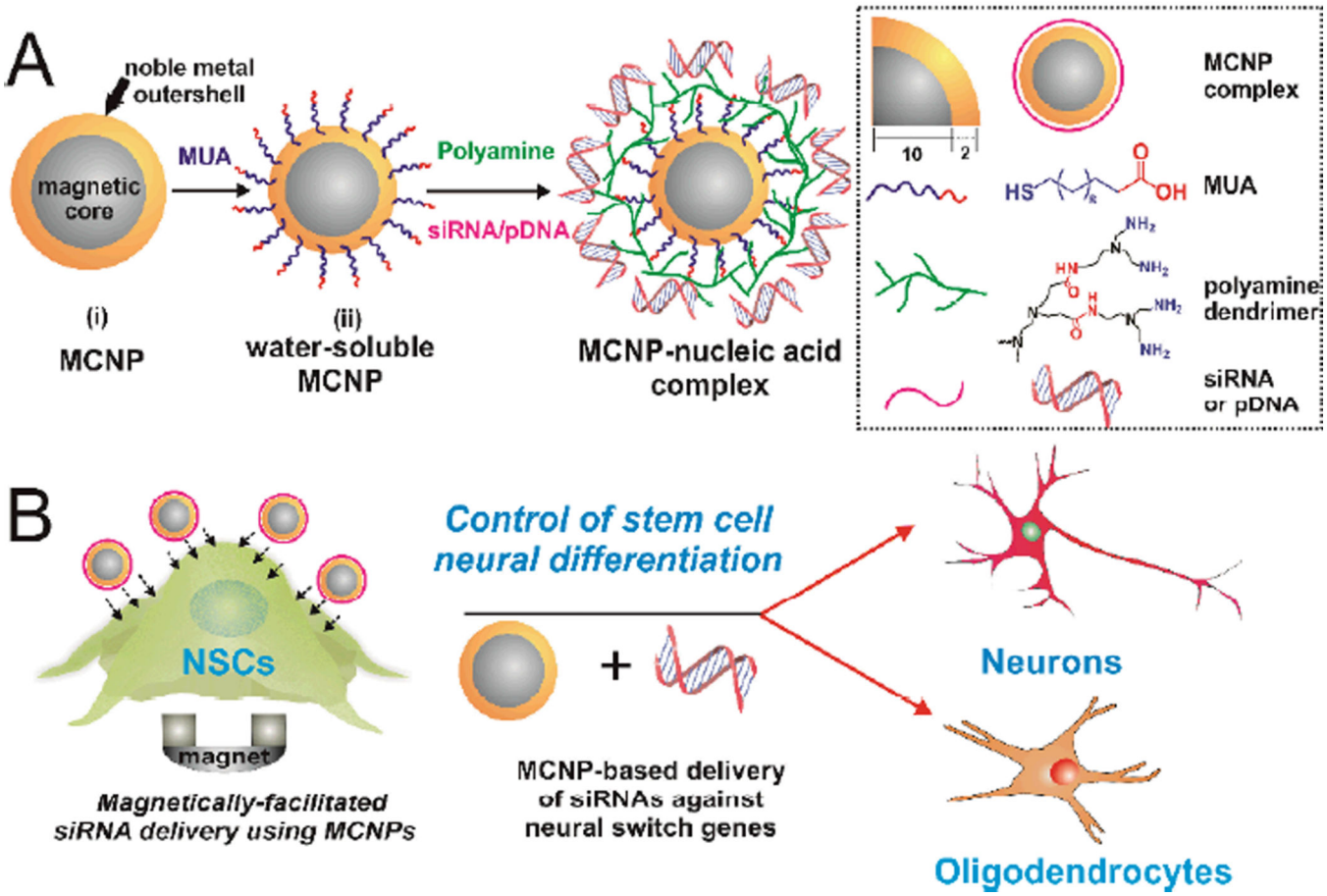

Figure 1.

General schematic diagram of our NP synthesis and their application for the differentiation of stem cells. **A)** Schematic illustration of generating non-water-soluble MCNPs and watersoluble MCNPs.**B)** Magnetically-facilitated siRNA delivery using MCNPs to control the differentiation of stem cells.

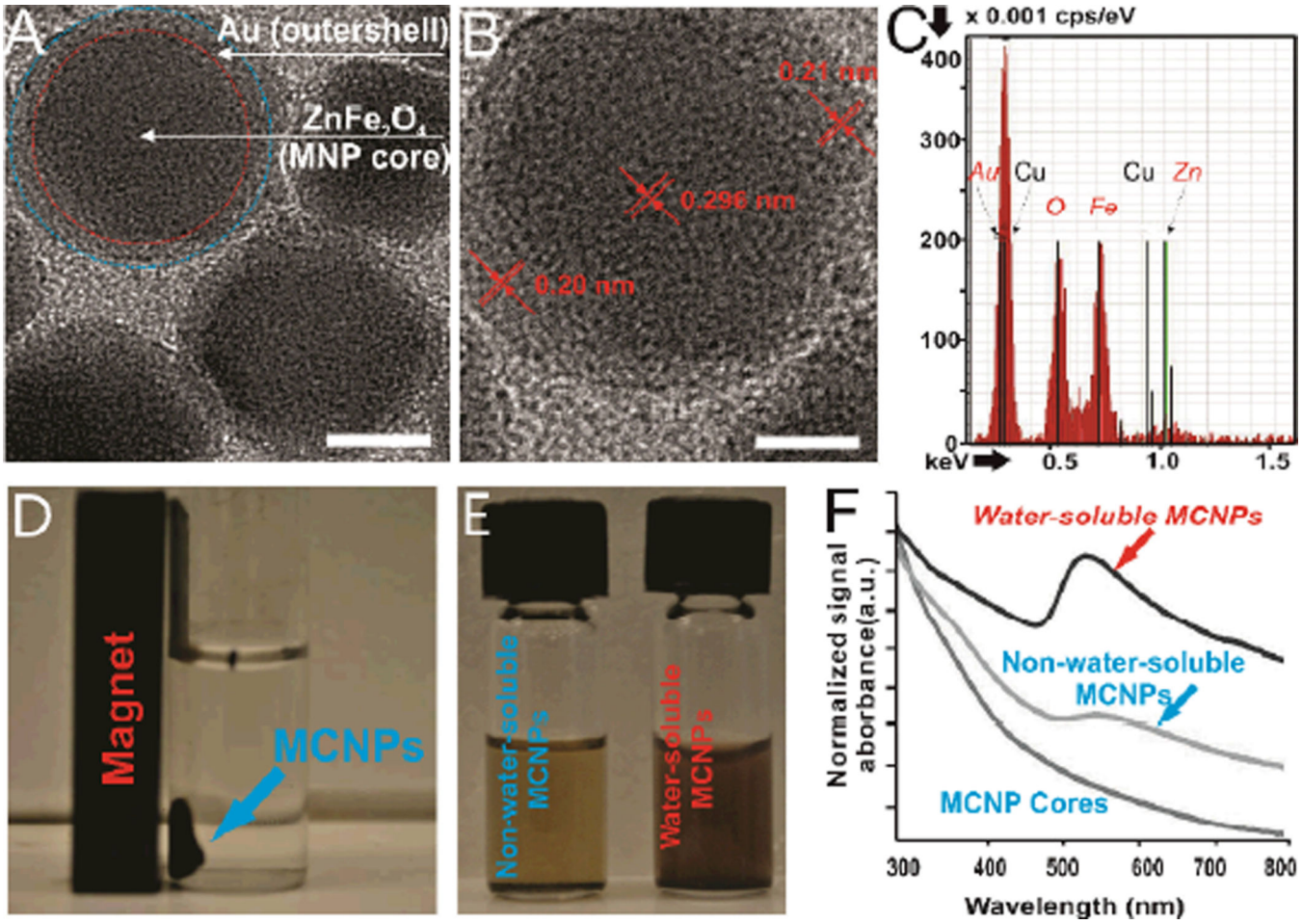

Figure 2.

A)TEM image of the MCNPs. Scale bar = 10 nm, **B)** HRTEM image of a single MCNP. Scale bar = 5 nm, **C)** EDAX spectra of individual MCNPs, **D)** Representative picture depicting that the MCNPs dispersed in water are attracted to a magnet. **E)** Representative picture of non-water-soluble and water-soluble MCNPs in solution. Please note that the light pink color of watersoluble MCNPs indicates the formation of a gold shell. **F)** UV-Vis absorption spectra of the MCNP cores, non-water-soluble MCNPs and water-soluble MCNPs. The cores and non-water-soluble MCNPs were dissolved in chloroform before UV-Vis analysis.

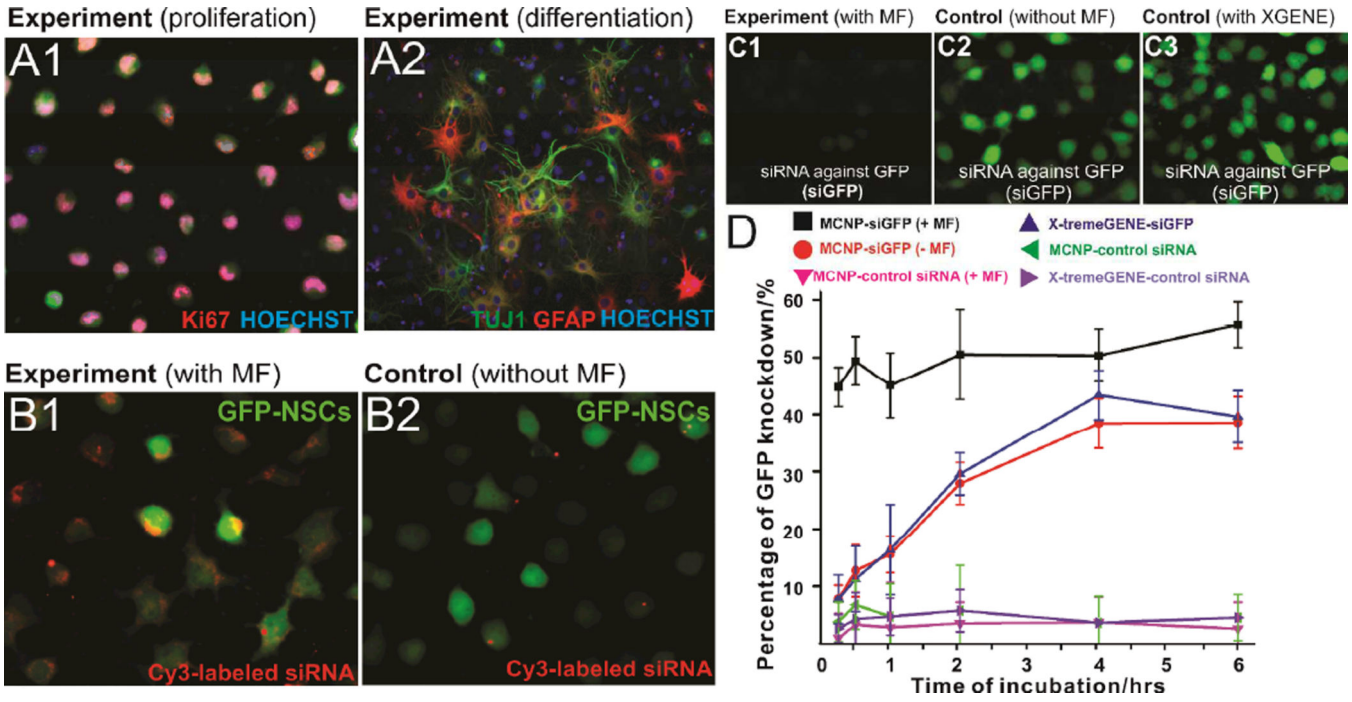

Figure 3.

A) Immunostaining data showing the proliferation (A1) and differentiation (A2) capability of NSCs after treatment with MCNPs (MCNPs, 5 μg/mL; negative control siRNA, 200 nM) in the presence of magnetic field (MF). The NSCs were stained with Ki67 as a proliferation marker and with TUJ1 (neurons) and GFAP (astrocytes) as differentiation markers. The nucleus was stained with Hoechst. **B)** Effect of presence (B1) and absence (B2) of MF on uptake of MCNP-Cy-3 labeled siRNA (MCNPs, 5 μg/mL; Cy-3 labeled siRNA, 200 nM) complexes in the NSCs. **C)** Knockdown of GFP fluorescence signal in NSCs treated with MCNPs-siGFP complexes in the presence (C1) or absence (C2) of an external magnetic field. The knockdown efficiency using MCNPs was compared to that using X-TremeGENE® (C3) as a positive control. The concentrations of MCNPs and siGFP were 5 μg/mL and 200 nM respectively. The amount of X-TremeGENE® used was within the manufacturer recommended range. The cells were exposed to the magnetic field for an optimum period of 30 min. **D)** Quantification of time-dependent GFP knockdown efficiency in NSCs using MCNPs [w/ or w/o magnetic field (MF)] and X-TremeGENE® complexed with either siGFP or control siRNA. As described in part C, the concentrations of MCNPs and siGFP were 5 μg/mL and 200 nM respectively.

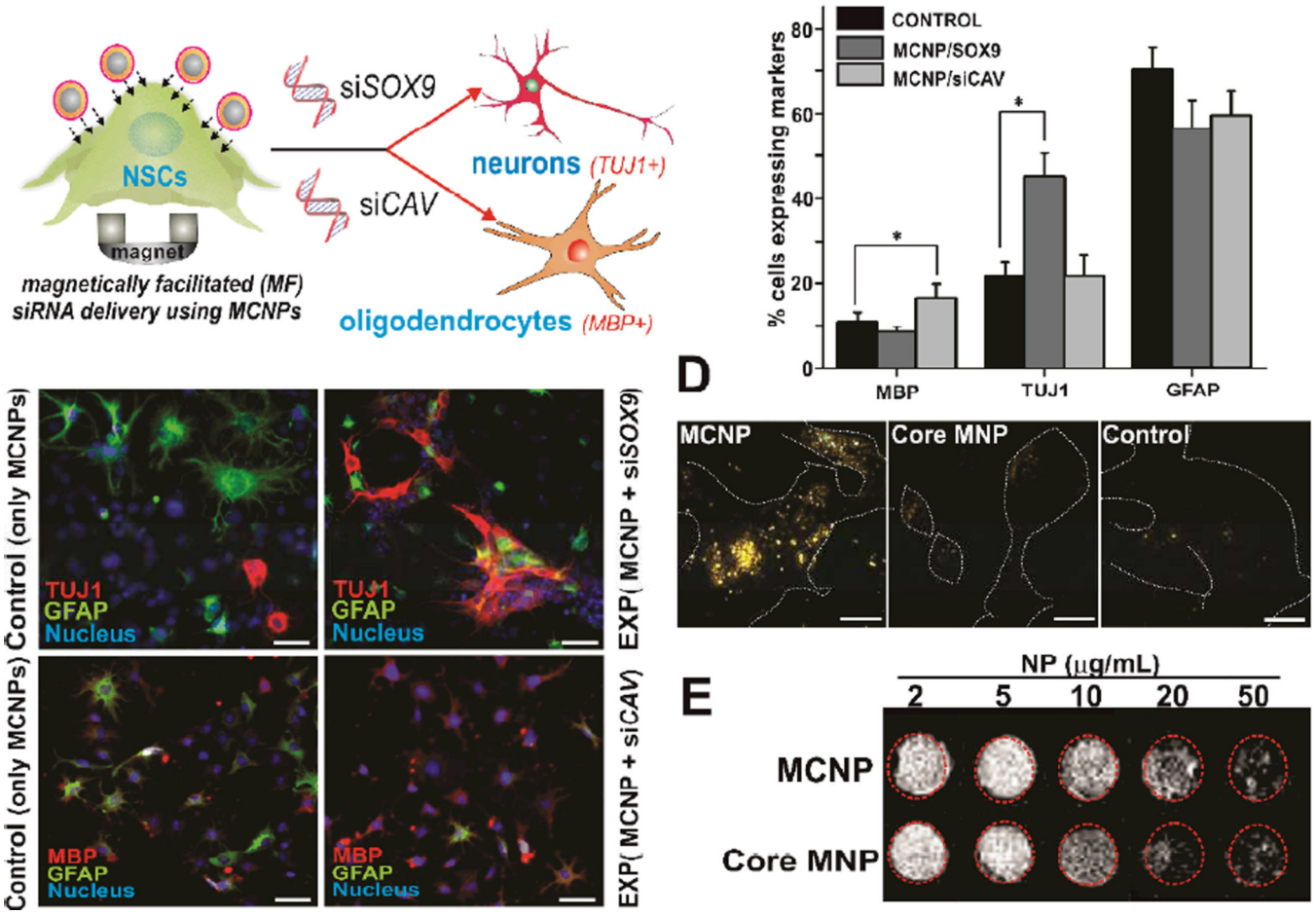

Figure 4.

A)MCNP-mediated magnetically-facilitated delivery of siRNA against *SOX9* (si*SOX9*) and *CAVEOLIN-1* (si*CAV*) for inducing neural differentiation of NSCs. **B)** Fluorescence microscopy images depicting neuronal (top row) and oligodendrocyte differentiation (bottom row) of the NSCs following delivery of si*SOX9* and si*CAV* respectively using MCNPs. The NSCs were stained with MBP (oligodendrocytes) and GFAP (astrocytes) in the case of MCNP/si*CAV* treated cells and for TUJ1 (neurons) and GFAP (astrocytes) in case of MCNP/si*SOX9* treated cells on day 7 of transfection. The nucleus was stained with Hoechst. Scale bar is 1 μm **C)** Quantification of percent cells expressing neural markers when treated MCNP/siCAV and MCNP/siSOX9 as compared to untreated cells. All results represent the average mean of three independent experiments. Values are represented as mean ± SD.*denotes $p < 0.001$ for neuronal differentiation and **denotes $p < 0.01$ for oligodendrocyte differentiation. **D)** Dark-field light scattering images for NSCs treated with MCNPs, Core ($ZnFe_2O_4$) MNPs and untreated NSCs (Control). Please note that the dark-field scattering signals from the core MNP and control experiments come from background signal due to cellular components. Scale bar is 100 nm. **E)** Signal intensity T2 weighted MR images of MCNP and Core NPs in phantom agar gel at 2–50 μg/ml concentration at 25 °C.